A Facile Strategy for Electrochemical Analysis of Chrysophanol Based on Nitrogen-Doped Graphene Supported ZnO Nanorods/Au Multihybrid Nanoarchitecture

Ling Shi[1,2], Zefeng Wang[1,2,*], Na Wu[1,2], Xianlan Chen[1,2], Guangming Yang[1,2,*], Wei Liu[1,2,*]

[1] School of science, Honghe University, mengzi, Yunnan 661199, PR China
[2] Key Laboratory of Natural Pharmaceutical & Chemical Biology of Yunnan Province, Mengzi, Yunnan 661199, PR China
[*]E-mail: wangzefeng841006@163.com, yangguangmingbs@126.com, liuwei4728@126.com

For the first time, N-doped reduced graphene oxide supported ZnO nanorods loading Au nanoparticles (N-rGO-ZnO-Au) multihybrid nanoarchitecture are successfully achieved via a simple strategy. N-rGO served as a large support material can disperse ZnO nanorods, and the abundant active sites of ZnO are benefit for growing Au NPs. The obtained mutihybrid nanoarchitectured materials are clearly characterized by transmission electron microscopy (TEM), X-ray photoelectron spectroscopy (XPS) and X-ray diffraction (XRD). The electrochemical behaviors and reaction mechanism of fabricating sensor toward chrysophanol (CHR) are investigated. The fabricated electrochemical sensor possesses excellent electrochemical characteristics for detecting of CHR. The peak current is proportional to CHR concentration in the range from 1.57 to 27.53 μM, the detection limit is 0.49 μM. Moreover, the suggested electrochemical sensor also show good reproducibility, stability and selectivity, and has been used to detect CHR in real sample.

1. INTRODUCTION

Chrysophanol (CHR) is one of the major anthraquinone and is an active ingredient of medicinal plant rhubarb [1, 2]. It is reported that the CHR has strong anti-fibrotic, anti-cancer action, anti-inflammatory activity, and anti-microbial activity, which usually used to therapy of gastrointestinal obstipation, indigestion, jaundice and diarrhea in Chinese clinics [3, 4]. Therefore, detection of the content of CHR in plant rhubarb is of extremely important for the quality control of medicinal herb and its products. It is very urgent that construct a sensitive, precise, and simple analytical method to detect

CHR in Chinese traditional medicines in clinical analysis. At present, some analytical methods have been applied for determination of CHR, for example, gas chromatography-mass spectrometry [5], high-performance liquid chromatography [6], and capillary electrochromatography [7]. Nevertheless, these analysis technologies usually have complex pretreatment procedures, intricate operate process, long-time detection, and expensive apparatuses. The electrochemical analysis technology has attracted much attention due to instrument simplicity, easyto-operate, low cost, fast response and excellent sensitivity [8, 9].

Recently, multifunctional nanomaterials that made up of different components are received great research interest due to the good electrochemical activity of obtained composites nanomaterials. The properties of composite material are not usually attainable in single material. It is well known that the electrochemical property of nanomaterials is strongly dependent on the structures of prepared nanocomposites which can increase mass and electron transport rate of target molecules. ZnO nanostructure has received exceptional attention among numerous nanomaterials because of its large specific surface area, excellent biological compatibility, excellent electron mobility, high catalytic efficiency, and non-toxicity, chemical stability, electrochemical activity [10, 11], which has been widely applied in biosensor field. For example, zhou et al [12] prepared gold nanoparticles loading well-arranged ZnO nanorods-reduced graphene oxide which show excellent electrochemical and photoelectrochemical performance for glucose. Gasparotto [13] prepared ZnO nanorods-Au nanoparticles nanohybrids which show a sensitive electrochemical response for detection of CA125/MUC126. Pruna et al [14] prepared ZnO nanorod core and polypyrrole shell arrays use electrochemical deposition and the obtained core-shell arrays possesss good electrochemical properties. Furthermore, ZnO is known as an excellent multifunction nanomaterial due to its the abundant active sites, which can be efficiently bonded with a variety of metal nanoparticles (NPs) and supporting materials such as graphene, carbon nanotube, Au NPs, Ag NPs, and so on.

Graphene as a star material has been widely used in electrochemical field due to its variety of excellent performance. And the introduction of nitrogen into the graphene structure can effectively improve the properties of obtained nanomaterials due to the introduction of nitrogen can effectively change elemental composition, which produces considerable number of defects into its lattice on the graphene surface. On the other hand, Au NP has received extensive research interest owing to its outstanding catalytic activity and good conductivity. It is well known that the Au NPs are known as an effective material for recognition biological molecules and show large potential for the signal amplification of biosensing [15, 16].

Based on the above considerations, we design a simple strategy to synthesize ZnO nanorods, then Au NPs are dispersed onto the surface of ZnO nanorods obtained ZnO nanorods loading Au NPs (ZnO/Au). And then ZnO/Au NPs are grown onto the surface of N-doped reduced graphene oxide obtained N-rGO-ZnO-Au multihybrid nanoarchitecture. The obtained N-rGO-ZnO-Au is used to fabricate electrochemical sensor for determination of CHR. The detection conditions are further investigated including electrochemical reaction mechanism and electrochemical activities toward CHR.

2. EXPERIMENTAL

2.1 Materials

HAuCl$_4$ was purchased from Shanghai Sybridge Chemical reagent Company. Nitrogen doped reduced graphene oxide was purchased from Nanjing Jcnano Technology Co., Ltd (China). Zinc acetate dihydrate (Zn(CH$_3$COO)$_2$·2H$_2$O), chloroauric acid (HAuCl$_4$.4H$_2$O), Methanol (99.5%), potassium hydroxide, trisodium citrate and CHR were obtained from Shanghai Chemical Reagent Co. Ltd. (Shanghai, China). CHR was dissolved into ethanol to prepare 4 mg mL^{-1} standard solution and stored in the fridge at 4 °C. The ultrapure water obtained by Milli-Q plus water purification system (Millipore Co. Ltd., USA) in all experiment.

2.2 Apparatus

The the sizes and morphology of the obtained nanomaterials are characterized with transmission electron microscope (TEM, JEM-2100, JEOL, Japan). X-ray diffraction (XRD, X'Pert^3 powder diffractometer, PANAlytical Company) is used to characterize crystal structures and phase composition of as-prepared nanomaterials. X-ray photoelectron spectroscopy (XPS) experiments are performed on a *K-Alpha$^+$* spectrometer (Thermo fisher Scientific) with Al Kα radiation (hν = 1486.6 eV). Electrochemical experiments are carried out on CHI 660E electrochemical workstation (CHI, Shanghai). A standard three electrode system, consisting of a nanomaterials-modified glass carbon electrode (GCE, 3mm diameter) as working electrode with a platinum wire counter electrode and Ag/AgCl electrode reference electrode are used throughout the experiment.

2.3 Synthesis of ZnO Nanorods

ZnO nanorods are synthesized according to the route reported in the literature but with some modification [17, 18]. Zinc acetate (4.45 mmol) is dissolved in 42 mL of methanol and 250 μL of ultrapure water in a flask. Then the solution is vigorous stirring at 60 °C. KOH (9.62 mmol, 82.0%, wt %) is dissolved in 23 mL methanol. And then obtained KOH solutions are added to the stirred above solution over 10-15 min. The reaction mixture is kept reacting for 135 min. The resultant solution became white and cloudy, cooled to room temperature, and then nitrogen purging is used to condense the original solution to 10 mL and the solution become clear again. It's been reported that condensing is benefit for increasing the ZnO nanorods growth rate [18, 19]. The condensed solution is aged for 12 h in bath at 60°C. The upper solution of the resulting white suspension is removed after 30 min. Then 50 mL of methanol is added into the above solution and stirred for 5 min. The obtained upper solution is removed again after 30 min. This process is repeated twice. And the upper fraction of the solution is taken away after overnight staying. Finally, the obtained solution is redispersed in methanol.

2.4 Preparation of ZnO/Au Nanoparticles

Before Au nanoparticles are assembled onto the surface of ZnO nanorods *via* in situ reduction, the obtained ZnO nanorods solutions are first dispersed in diluted trisodium citrate aqueous solution and ultrasonicated to form a 0.4 mmol/L suspension (50 mL). Then $HAuCl_4$ (10 mL, 0.39 mM) is added dropwise into ZnO solution under vigorous stirring. The color of the solution is changed from white to lilac after reaction for 12 h at room temperature. The obtained product is then collected by centrifugation and washed with ultrapure water and ethanol several times.

2.5 Synthesis of N-rGO-ZnO-Au NCs multihybrid nanoarchitecture

In a typical procedure, 50 mL ZnO-Au NPs (3.0 mg/mL) and 10 mL N-doped graphene suspension (0.5mg/mL) are mixed under sonication (200 W) for 6 h.

2.6 Real Sample Assay

The sample preparation is performed as Ref. [20]. The traditional Chinese medicine of rhubarb is obtained from a local pharmacy. 50 mg of sample powder is extracted with 25 mL ethanol for 30 min by ultrasonic extraction. Then the extraction solution is isolated by centrifugation, the supernatant is collected. The obtained solution by diluted to 50.0 mL with ethanol for further analysis.

2.7 Preparation of electrode and analytical procedure

The bare GCE is thoroughly polished with Al_2O_3 (1.0, 0.3 and 0.05 µm), then sonicated successively in 1:1 nitric acid solution, ethanol and ultrapure water, and then dried with nitrogen gas. Then 7 µL 1 mg/mL of as-prepared ZnO, ZnO/Au, N-rGO-ZnO/Au suspension is dropped onto GCE and dried in air, respectively. Electrochemical impedance spectra (EIS) are performed using Autolab PGSTAT302N electrochemical workstation in 10 mM $Fe(CN)_6^{3-/4-}$ containing 0.1 M KCl with the frequency range from 0.01 Hz to 10 kHz. CV and DPV experiments are carried out in 0.1 M acetate buffer solutions containing a constant concentration of CHR. An accumulation method is carried out under open-circuit conditions before the CV and DPV measurement.

3. RESULT AND DISCUSSION

3.1 Characterization of as-prepared nanomaterials

In the process of preparing ZnO nanorods, Zinc acetate and potassium hydroxide are used as the initial reactant. The intermediate product of $Zn(OH)_2$ can be obtained at the initial stage. Since $Zn(OH)_2$ is less stable than ZnO, $Zn(OH)_2$ spontaneously transforms into ZnO products. After reacting a period of time, nitrogen purging is used to condense the original solution. It is reported that the condensing is benefit for growing of ZnO nanorods. The obtained ZnO nanorods are well dispersed in

methanol solvent. TEM and HRTEM are employed to characterize the structural features of ZnO nanorods. Figure 1A reveals that the prepared ZnO possesses a good rodlike structure. Most of ZnO nanorods are aligned uniaxially parallel to each other. The average length of nanorod is as long as 25 nm. The results further show that the nanorods grow further along their c axis forming longer rods. The HRTEM are clearly revealed that the two lattice planes with the interplanar distances of 0.25, and 0.19 nm correspond well to (101) and (102) planes of ZnO.
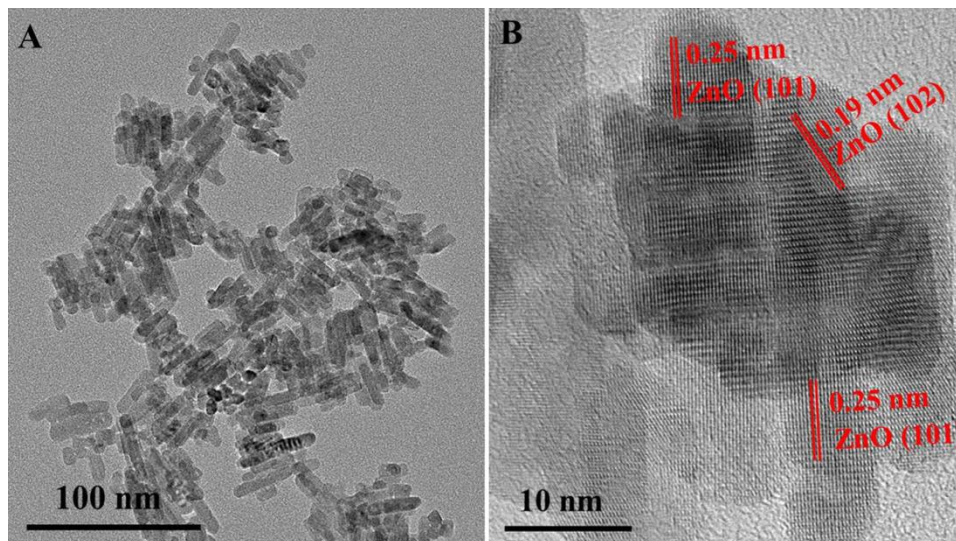
Figure 1. TEM (A) and HRTEM (B) image of ZnO nanorods.
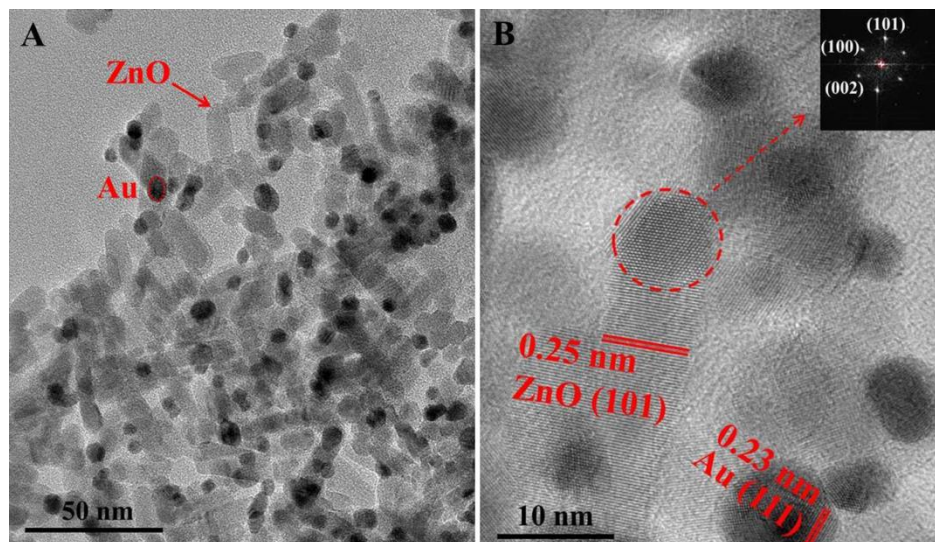
Figure 2. TEM (A) and HRTEM (B) image of ZnO/Au nanoparticles. Inset image is FFT pattern of the HRTEM image shown in panel B (circled part).

Next, Au NPs are deposited on ZnO nanorods surface to prepare ZnO/Au nanoparticles *via* in situ reduction with trisodium citrate. Figure 2 A and B show that the ZnO nanorods are decorated with nanosized Au NPs. The HRTEM image of the ZnO/Au nanoparticles shows that the average size of Au NPs is 18 nm. The d-spacing value is 0.23 nm prove that the obtained Au NP is face-centered cubic

(fcc). And the d-spacings of the adjacent fringe for the ZnO nanocrystals are 0.25 nm, which is indexed to the (101) crystalline plane. While the fast Fourier transform (FFT) pattern (Figure 2B, inset) of the HRTEM image (circled part, Figure 2B) further indicates that the ZnO nanorod is a single crystal.

The structure and morphology of N-rGO-ZnO/Au multihybrid nanoarchitectures are clearly revealed by the TEM and HRTEM images in Figure 3. A transparent and flake-like monolayer graphene sheets can be clearly observed from Figure 3A. And few agglomerated of ZnO/Au nanoparticles are dispersed onto the surface of N-rGO. The results further reveal that N-doped graphene is well kept after loading ZnO/Au nanoparticles. Moreover, the ZnO/Au nanoparticles grown onto the surface of N-rGO surfaces can effectively prevent the N-rGO from aggregating and restacking. Figure 3B shows that the d-spacing is 0.23 nm, which show fcc of Au NPs. And the interplanar spacing for ZnO is 0.25 nm, which is assigned to the (101) crystalline plane of the Pt lattice.
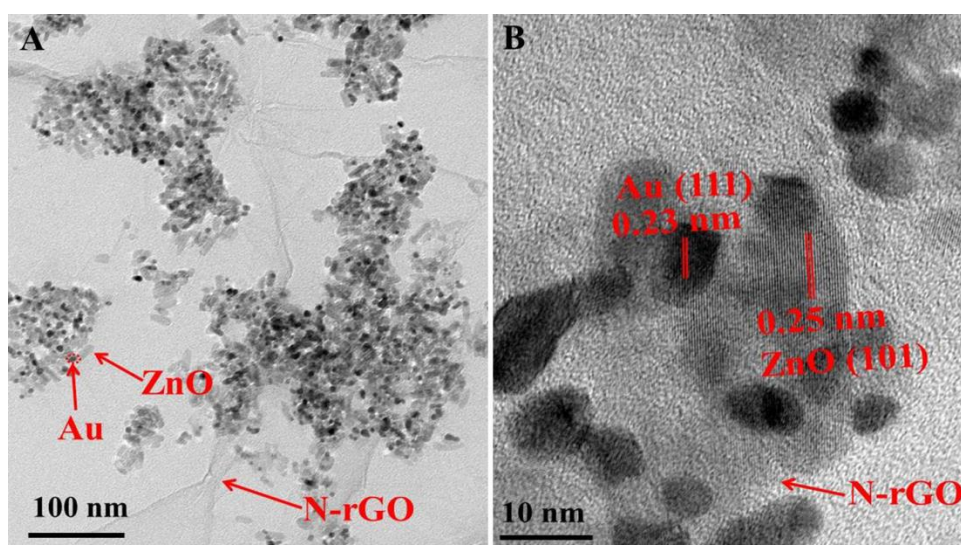
Figure 3. TEM (A) and HRTEM (B) image of N-rGO-ZnO/Au multihybrid nanoarchitectures.

XRD analysis is carried out to detect the internal lattice of prepared nanomaterials. Figure 4 shows the XRD patterns of ZnO nanorods, ZnO/Au and N-rGO-ZnO/Au nanomaterials. In the case of ZnO (curve a), the diffraction peaks at 31.80° (100), 34.46° (002), 36.36° (101), 47.64° (102), 56.56° (110), 62.86° (103), 68.04° (112), 72.43° (004), and 77.07° (004) that are also in accordance with the hexagonal wurtzite structure of ZnO according to the JCPDS standard card no. 36-1451 [21, 22]. Figure 4b shows the XRD patterns of ZnO/Au, the diffraction peaks at 38.25° and 44.42° are corresponded to the (111) and (200) facets, respectively. Figure 4c shows the XRD patterns of N-rGO-ZnO/Au multihybrid nanoarchitectures, the peak around 22.64° shows the typical diffraction peak of the (002) plane in hexagonal graphite. And the characteristic diffraction peaks of Au NPs and ZnO nanorods are also can be observed, indicating that ZnO/Au are fully decorated on N-rGO.
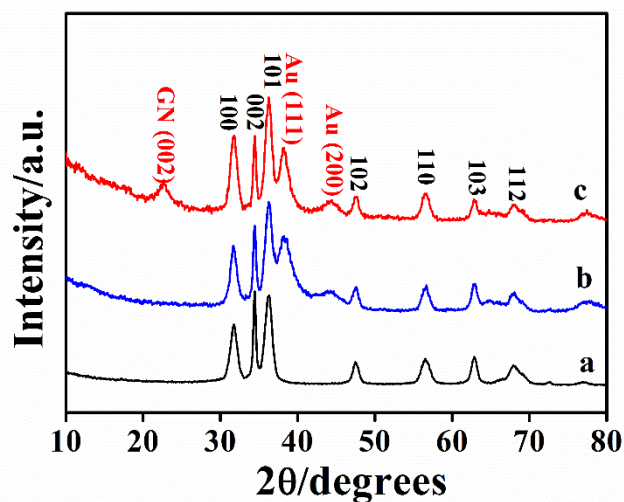
Figure 4. XRD patterns of (a) pure ZnO nanorods sample, (b) ZnO/Au and (c) N-rGO-ZnO/Au multihybrid nanoarchitectures.

In order to further investigate the chemical composition and states of as-prepared N-rGO-ZnO/Au, the XPS analysis has been operated. From Figure 5A, the existence of Au, C, N, O, and Zn peak in survey spectrum, the formation of N-rGO-ZnO/Au multihybrid nanoarchitectures can be demonstrated. The spectrum of C1s can be deconvoluted into sp^2 C (C=C) centered at 284.5 eV, sp^3 C (C-C and C-N) centered at 285.8 eV, C=O centered at 287.0 eV, and O-C=O centered at 289.0 eV, respectively (Figure 5B) [23, 24]. The presence of C-N clearly reveals the existence of C and N ingredients. In Figure 5C, the deconvolution of N 1s spectra displays two peaks centered at 399.1 eV (-NH-) and 400.4 eV (-N^+-) [25]. Figure 5D displays the high-resolution XPS spectra of O 1s can be deconvoluted into four species centered at 530.0, 531.0, 532.2 and 533.2 eV. The peak at 530.0 eV is attributed to the bonding between O^{2-} and metal ions in würtzite ZnO (O_L), the peak centered at 531.0 eV is comes from the oxygen vacancies (O_V), the peak at 532.2 eV is corresponds to the C-O. The high energy is represented to the chemisorbed and dissociated oxygen species (O_C) which may originate from the OH groups due to the water adsorption in synthesizing materials [26, 27]. It is reported that ZnO shows an n-type property due to the defect and oxygen vacancies [28]. Notably, the defect and vacancies will benefit for loading Au nanoparticles. Figure 5E shows the high-resolution Zn 2p region, the binding energy centered at 1022.2 eV and 1045.3 eV are attributed to the Zn $2p_{3/2}$ and Zn $2p_{1/2}$, respectively. And the energy separation is 23.1 eV, which is typical for ZnO [29]. Figure 5F shows the Zn 3p and Au 4f core-levels for N-rGO-ZnO/Au nanomaterials, two pair of clear binding energy peaks are observed. The binding energy at 84.2 and 87.8 eV can be rationalized to Au(0) $4f_{7/2}$ and Au(0) $4f_{5/2}$ electronic states, respectively. These values corroborate that Au NPs in the N-rGO-ZnO/Au are predominantly metallic. Moreover, the obvious diffraction peak alongside Au 4f region can be attributed to the characteristic peak of Zn 3p. The two peaks centered at 89.5 and 92.1 eV are attributed to the presence of Zn $3p_{3/2}$ and Zn $3p_{1/2}$, respectively [29].
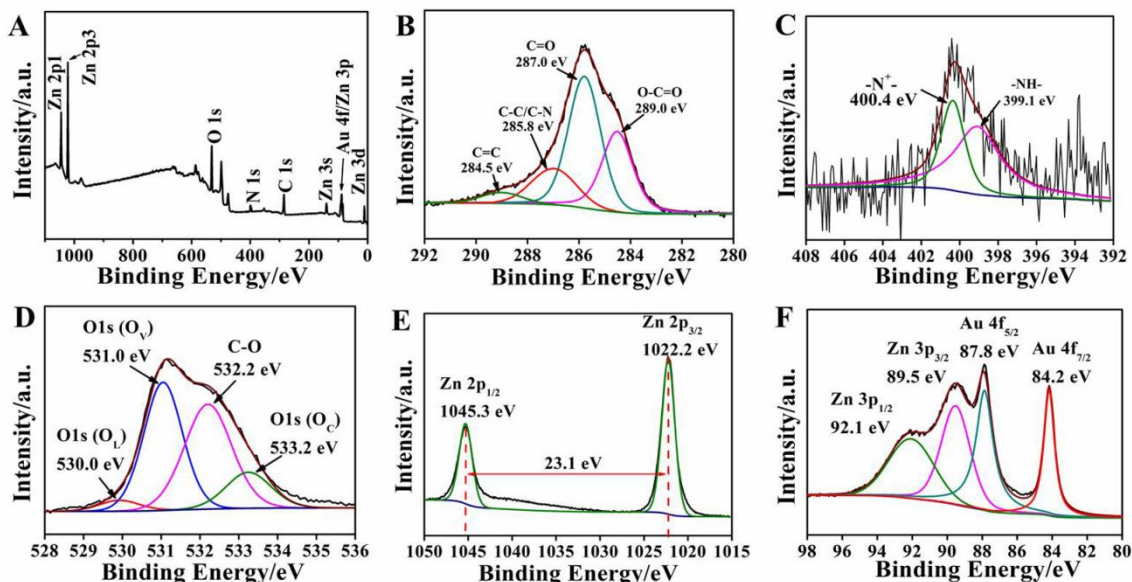
Figure 5. (A) XPS survey spectra of N-rGO-ZnO/Au multihybrid nanoarchitectures and high resolution spectra of (B) C 1s, (C) N 1s, (D) O 1s, (E) Zn 2p, (F) Zn 3p and Au 4f.

3.2 Electrochemical Surface characterization of modified electrode

The electrochemical behavior of ZnO/GCE, ZnO/Au/GCE and N-rGO-ZnO/Au/GCE are investigated by CV in Fe^{3+}/Fe^{2+} system. The results are shown in Figure 6A. In the comparison, N-rGO-ZnO/Au/GCE exhibits a good defined redox peak. The peak current is obvious higher than the other and the peak to peak separation value ($\triangle Ep$) is smaller than the other.
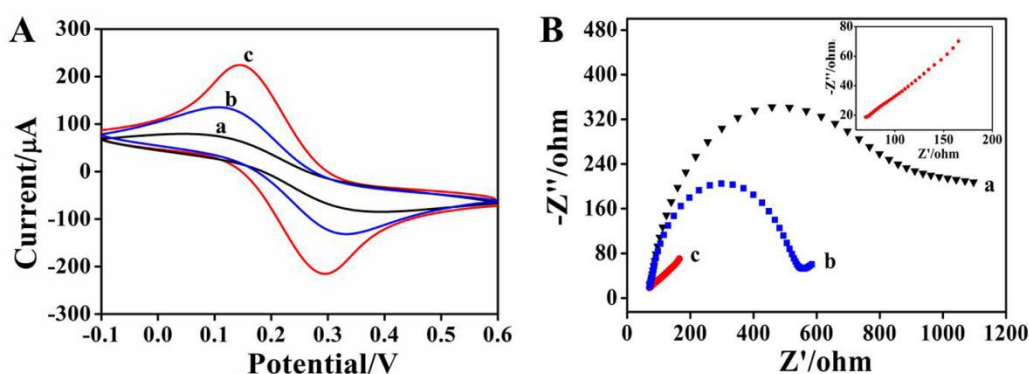
Figure 6. CVs (A) and EIS (B) of ZnO/GCE (a), ZnO/Au/GCE (b) and N-rGO-ZnO/Au/GCE (c) in 1.0 mM $Fe(CN)_6^{3-/4-}$ solution containing 0.5 M KCl. Scan rate: 50 mV/s.

The result implies that N-rGO-ZnO/Au/GCE has better electron transfer rate compared with other modified electrode. Furthermore, EIS is used to study the interfacial electron transfer properties of surfaces in 1.0 mM $Fe(CN)_6^{3-/4-}$ solution containing 0.5 M KCl. The diameter of the semicircle is a good measure of the resistance of the electrode. From Figure 6B, we can see that the ZnO/GCE and ZnO/Au/GCE have a higher charge transfer resistance values. And the charge transfer resistance

values further decreased when modified GCE with N-rGO-ZnO/Au multihybrid nanoarchitectures. These results imply that the combination of N-rGO, ZnO and Au NPs could enhance effectively electrical conductivity due to the synergistic effects of N-rGO, ZnO and Au NPs. So the N-rGO-ZnO/Au multihybrid nanoarchitectures can facilitates effectively charge transfer and maybe benefit for detecting CHR.

3.3 Electrochemical Behavior of CHR on modified electrode

The electrochemical behavior of CHR is investigated on modified electrodes using CV. Figure 7 shows the CVs of ZnO/GCE, ZnO/Au/GCE and N-rGO-ZnO/Au/GCE in 0.1 M acetate buffer solutions (pH=3.6) containing 10.18 μM CHR at a scan rate of 20 mV s^{-1}. The ZnO/GCE and ZnO/Au/GCE exhibit a poor response to CHR. And a pair of well redox peaks is obtained when modified with N-rGO-ZnO/Au multihybrid nanoarchitectures. Meantime, the △Ep value is lowest than the ZnO and ZnO/Au modified electrode.
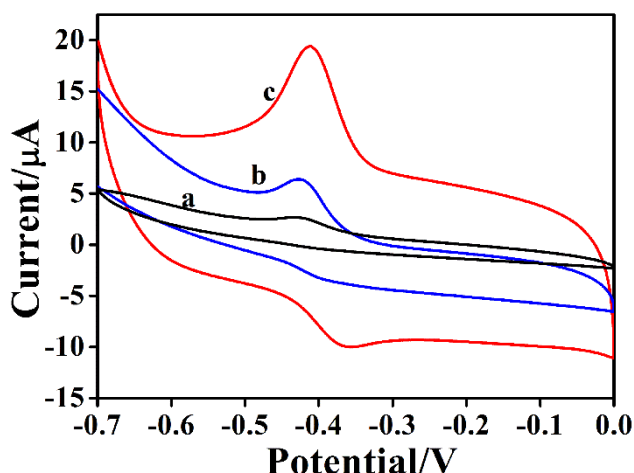
Figure 7. (A) CV response of ZnO (a), ZnO/Au (b) and N-rGO-ZnO/Au (c) modified electrodes in the presence of 10.18 μM CHR in 0.1 M pH=3.6 acetate buffer solutions at a scan rate of 20 mV s^{-1}. Accumulation is performed under open-circuit for 6 min.

The results imply that the prepared N-rGO-ZnO/Au can effectively facilitate the electron transfer of CHR due to the synergistic effects from N-rGO, ZnO and Au NPs. The prepared N-rGO-ZnO/Au possesses excellent electrocatalytic activity may be ascribed the following reasons: Firstly, N-rGO has large surface area which is benefit for adsorbing CHR. Secondly, ZnO nanorods possess excellent biological compatibility and high catalytic efficiency which can promote the direct electron transfer between CHR and electrode [30]. Thirdly, Au NPs can offer a large sensing platform for the recognition of CHR. Furthermore, Au NPs also can enhance electron transfer between electrode and CHR molecules. These excellent performances can be synergistically enhancement. The CHR can be effectively detected based on the excellent electrocatalytic activity of obtained N-rGO-ZnO/Au multihybrid nanoarchitectures.

To further investigate the electrode reaction of CHR, the influence of scan rate on the redox of CHR is studied by CV. Figure 8A shows the CVs observed for the electrochemical oxidation of CHR at N-rGO-ZnO/Au/GCE for different scan rates (10-250 mV s^{-1}). We can see that the redox peak currents are linearly increased with the increasing of scan rate. Figure 8B reveals that the redox peak currents of CHR are linearly proportional to square root of the scan rate ($v^{1/2}$). The regression equations of $I_{pa} = 5.7927v^{1/2}+13.8739$ ($R^2=0.9913$) and $I_{pc} = 6.2841v^{1/2}-3.6267$ ($R^2=0.9967$). These results suggest that the oxidation of CHR at N-rGO-ZnO/Au modified electrode is diffusion-controlled [31]. Figure 8C displays that the anode (E_{pa}) and cathode (E_{pc}) peak potential have good linear relationships with the napierian logarithm of scan rate (lnv).
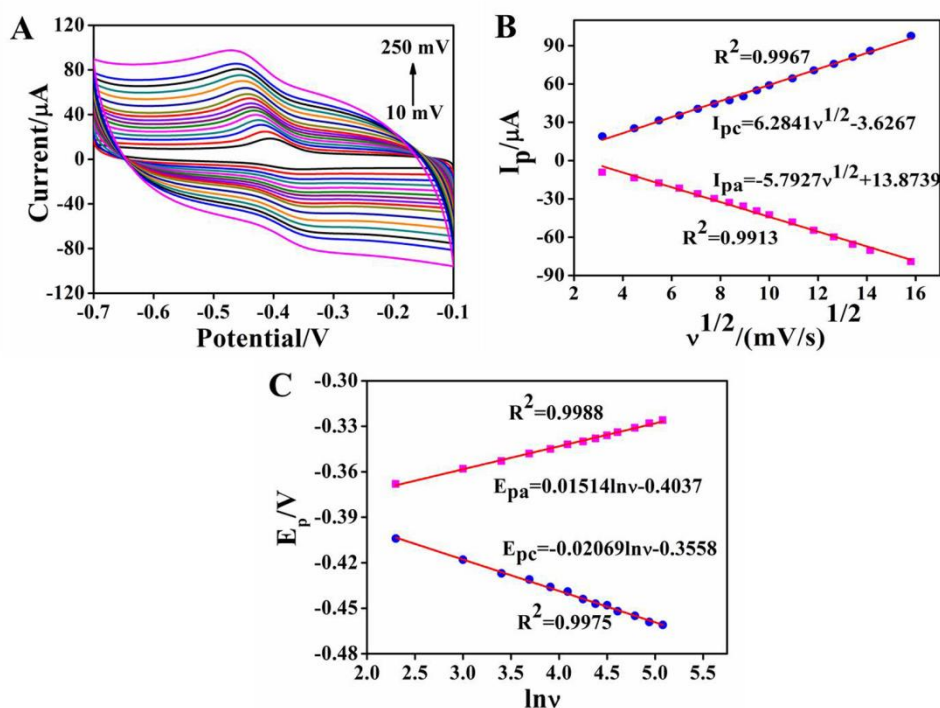
Figure 8. (A) CVs of N-rGO-ZnO/Au/GCE in pH = 3.6 acetate buffer solutions containing 10.18 μM CHR at scan rate of 10, 20, 30, 40, 50, 60, 70, 80, 90, 100, 120, 140, 160, 180, 200, and 250 mV s^{-1} (from inner to outer curve). (B) Calibration plots of cathodic and anodic peak current versus square root of scan rate. (C) Plots of anodic and cathodic potentials against the lnv.

The regression equation is $E_{pa}=0.01514lnv-0.4037$, $R^2=0.9988$ and $E_{pc}=-0.02069lnv-0.3558$, $R^2=0.9975$. According to the Laviron equation [32], the electron transfer rate constant (k_s), electron transfer number (n), and charge transfer coefficient (α) can be calculated. Here, the slope value from the plot of anodic peak potential (E_{pa}) versus lnv is equal to $RT/(1-\alpha)nF$ and the slope value from the plot of cathode peak potential (E_{pc}) versus lnv is equal to $RT/\alpha nF$, respectively.

$$E_{pa} = E^{0'} + \frac{RT}{(1-\alpha)nF} lnv \qquad \text{Eq. (A.1)}$$

$$E_{pc} = E^{0'} - \frac{RT}{\alpha nF} lnv \qquad \text{Eq. (A.2)}$$

$$\lg k_S = \alpha \lg(1-\alpha) + (1-\alpha)\lg\alpha - \lg\frac{RT}{nF\upsilon} - \alpha(1-\alpha)\frac{nF\Delta E_p}{2.3RT} \quad \text{Eq. (A.3)}$$

Where E_p is the peak potential, $E^{0'}$ is the formal standard potential, R indicates the universal gas constant (R=8.314 J mol^{-1} K^{-1}), T denotes the absolute temperature (T=298 K), F is the Faraday's constant (F=96485 C mol^{-1}), υ denotes the scan rate. According to the above equation, the value of n, α and k_s can be calculated is 2, 0.42 and 0.36 s^{-1}, respectively. Hence, these results imply that the electrochemical oxidation of CHR is two electron transfer process. And the results further prove that the electrochemical reaction is controlled by diffusion which in agreement with the results discussed above.

3.4 Optimization Conditions

The influence of pH is investigated towards the CHR oxidation at N-rGO-ZnO/Au/GCE using CV. Figure 9A demonstrates the CV curves obtained for oxidation of CHR at different pH acetate buffer solutions. It is observed that the peak current increased first and then decreased with the increasing of pH, and a pair of good redox peak can be obtained at pH=3.6 solution. Therefore, pH=3.6 is used as supporting electrolyte for further electrochemical experiments. Moreover, the redox peak potential of CHR is shifted negatively with the increasing of pH. Figure 9B reveals that a good linearity is obtained between peak potential and pH value. The linear equation of CHR is E_{pa}=-0.057pH-0.12 (R=0.9916), E_{pc}=-0.045pH-0.23 (R=0.9964), respectively. The slope of the calibration curve -0.057 V and -0.045 V are close to the theoretical value -0.0592 V, suggesting that the transferred electron number is equal to the number of protons [32]. Furthermore, based on the formula [33]: $dE_p/dpH = 2.303mRT/nF$, where n is the number of electron, m represents the number of proton. The m/n can be calculated is 0.95 and 0.75 for the oxidation and reduction processes, respectively. It shows that the number of electron and proton in the electrochemical reaction of CHR is equal [34]. Therefore, the electrochemical reaction of CHR on the N-rGO-ZnO/Au/GCE is a two-electron and two-proton process.
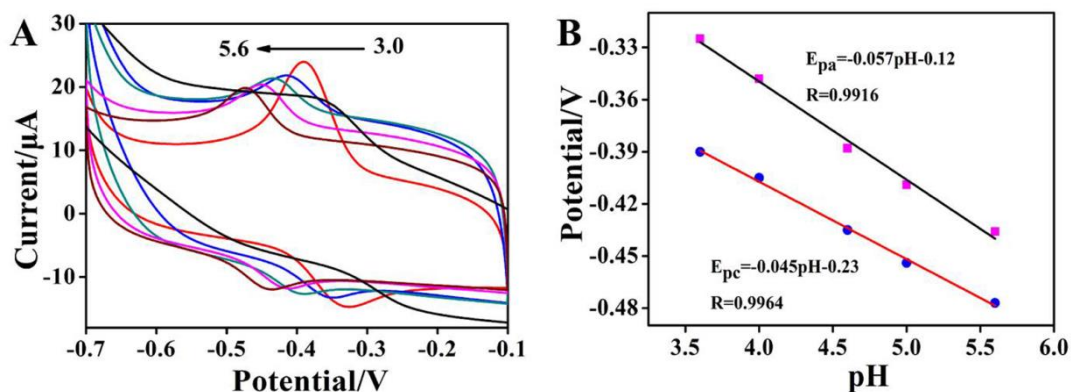
Figure 9. (A) CVs obtained at the N-rGO-ZnO/Au/GCE in acetate buffer solutions with different pH values (3.0, 3.6, 4.0, 4.6, 5.0, and 5.6) containing 10.18 μM CHR at scan rate of 20 mV s^{-1}. (B) The plots of cathodic and anodic peak potential of CHR versus pH values. Accumulation is performed under open-circuit for 6 min.

The amount of N-rGO-ZnO/Au/GCE is an important element for the recognition of CHR. The volume of N-rGO-ZnO/Au from 2 to 9 μL (with the concentration of 1.0 mg/mL) is investigated. As shown in Figure 10A, the peak current is gradually increased with the suspension volume from 2 to 7 μL and then tended to remain unchanged. It is maybe due to the increasing number of N-rGO-ZnO/Au on the GCE surface and improved ability to capture CHR. And overmuch suspension will lead to thicker film when increasing the amount of modifiers, which will obstruct the interface electron transfer. Thus, the optimal volume of 7 μL is employed in our experiments.
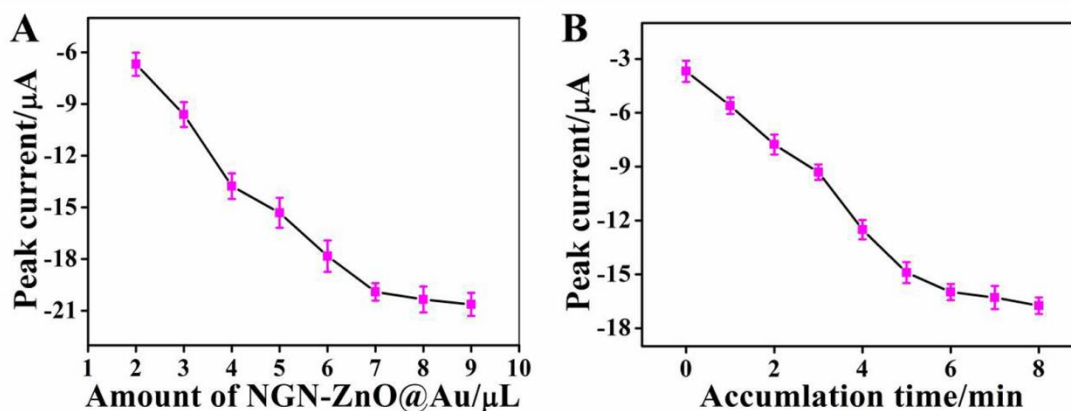
Figure 10. (A) The influence of the amount of N-rGO-ZnO/Au on oxidation peak current of 10.18 μM CHR. (B) Influence of accumulation time on the oxidation peak current of 10.18 μM CHR.

When considering the electrochemical reaction of CHR on N-rGO-ZnO/Au modified GCE, the accumulation time is also investigated by DPVs, the results are shown in Figure 10B. The oxidation peak currents increased gradually with the accumulation time increased from 0 min to 6 min indicates a great many of the CHR is adsorbed at the surface of GCE and thereafter the peak current tends to be almost unchanged proving that the adsorption equilibrium is reached. Therefore, 6 min is chosen for CHR accumlation.

3.5 Determination of CHR

The DPV technique is used to detect CHR at the N-rGO-ZnO/Au/GCE under optimal conditions. Figure 11A displays the DPV response for different concentration of CHR in pH=3.6 acetate buffer solutions. It is observed that the oxidation peak current increased linearly with the increasing of CHR concentration. As shown in Figure 11B, the oxidation peak currents are linear relationship with the CHR concentrations. The corresponding regression equation is $I_{pa}=-1.09c-1.47$ ($R^2=0.9968$). The linear range is 1.57 to 27.53 μM and detection limit is 0.49 μM (S/N=3). Obviously, the proposed sensor possesses excellent electrochemical performance maybe due to the unique structure and eminent catalytic activity of the N-rGO-ZnO/Au.
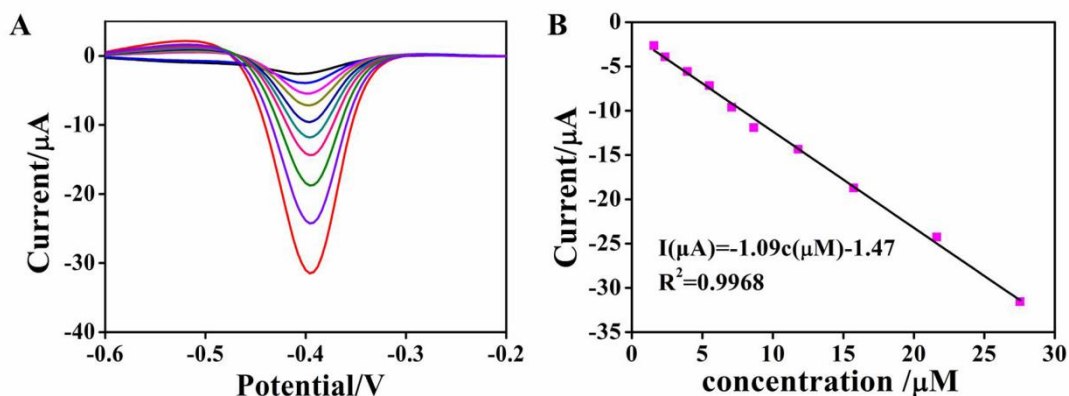
Figure 11. (A) DPV response of the N-rGO-ZnO/Au/GCE under optimum conditions for different CHR concentrations: 1.57, 2.36, 3.93, 5.51, 7.08, 8.65, 11.80, 15.73, 21.63, 27.53 µM. (B) The calibration curves of CHR.

3.6. Reproducibility, stability and selectivity studies

The reproducibility of the sensor is investigated using CV. Five N-rGO-ZnO/Au/GCEs fabricated using the same method are used for the determination of 10.18 µM CHR in pH=3.6 acetate buffer solutions. The results of reproducibility monitored show that the RSD value is 2.8% demonstrates the excellent reproducibility of N-rGO-ZnO/Au/GCE. The stability of proposed sensor is evaluated by CV measurements. The modified GCE is continuously detected for 30 consecutive days. The results show that the current response of sensor is almost no changed. Which confirm that the fabricated sensor has a good stability. Interference study is performed by adding some possible co-existing substances in pH=3.6 acetate buffer solutions containing 10.18 µM of CHR. The results show that 100-fold of NH_4^+, CO_3^{2-}, SO_4^{2-}, NO_3^{2-}, Cl^-, Ca^{2+}, Cu^{2+}, Zn^{2+} and Mg^{2+} did not show obvious interface. The results show that the fabricated sensor possesses good reproducibility, stability and selectivity.

3.7. Real sample analysis

Table 1. The recoveries of CHR from rhubarb samples (n=3).

	Original found/µM	Standard added/µM	Total founded/µM	Recovery/%
1	3.14	5.0	8.08	98.8
2	2.86	10.0	13.12	102.6
3	3.09	15.0	17.97	99.2

In order to evaluate the practical application of the proposed method, the proposed sensor is used to detect CHR in rhubarb by using standard addition method. The extraction solution is diluted 5 times before electrochemical experiments. The results are listed in Table 1. The content of CHR in rhubarb is calculated to be about 3.85 mg g^{-1}. The result is in consistent with the other detection

method reported in literature [6, 35]. The satisfactory recoveries are obtained from 98.8-102.6%, which indicate that fabricated electrochemical sensor is suitable for practical application.

4. CONCLUSIONS

In this work, we successfully prepared N-rGO-ZnO-Au multihybrid nanoarchitecture via a simple strategy. The obtained mutihybrid nanoarchitectured materials are clearly characterized by TEM, XPS and XRD. The proposed N-rGO-ZnO-Au is used to fabricate sensor for the electrochemical determination of CHR. The obtained N-rGO-ZnO-Au multihybrid nanoarchitectures possess an excellent electrocatalytic activity. The results show that the linear range is 1.57 to 27.53 μM with the detection limit of 0.49 μM. The proposed sensor display good selectivity, reproducibility and stability. Furthermore, the proposed sensor has good practical ability for the determination of CHR in rhubarb Chinese herbal medicines.

References

1. H. F. Zhang and Y. P. Shi, *Talanta*, 82 (2010) 1010.
2. J. Koyama, I. Morita and N. Kobayashi, *J. Chromatogr. A*, 1145 (2007) 183.
3. L. P. Ma, L. Zhao, H. H. Hu, Y. H. Qin, Y. C. Bian, H. D. Jiang, H. Zhou, L. u. S. Yu and S. Zeng, *J. Ethnopharmacol.*, 153 (2014) 864.
4. K. Chen, C. Q. Wang, Y. Q. Fan, Y. S. Xie, Z. F. Yin, Z. J. Xu, H. L. Zhang, J. T. Cao and Y. Wang, *International journal of clinical and experimental medicine*, 8 (2015) 10558.
5. Q. H. Chen, H. S. He, S. W. Luo, L. Xiong and P. Li, *J. Chromatogr. B*, 973 (2014) 76.
6. S. X. Feng, M. M. Li, D. Zhao, X. H. Li, L. Zhang, Z. Wang and N. N. Gao, *Chinese Herbal Medicines*, 9 (2017) 388.
7. H. X. Lü, J. B. Wang, X. C. Wang, X. C. Lin, X. P. Wu and Z. H. Xie, *J. Pharm. Biomed. Anal.*, 43 (2007) 352.
8. Z. F. Wang, G. Z. Gou, L. Shi, J. Yang, C. Xu, L. Zhang, A. P. Fan and Y. Min, *J. Appl. Polym. Sci.*, (2018) 4670.
9. E. M. Mximnano, F. D. Lima, C. A. L. Cardoso and G. J. Arruda, *Electrochim. Acta*, 259 (2018) 66.
10. R. Ahmad, N. Tripathy and Y. B. Hahn, *Biosens. Bioelectron.*, 45 (2013) 281.
11. S. K. Arya, S. Saha, J. E. Ramirez-Vick, V. Gupta, S. Bhansali and S. P. Singh, *Anal. Chim. Acta.*, 737 (2012) 1.
12. F. Zhou, W. X. Jing, S. Liu, Q. Mao, Y. X. Xu, F. Han, Z. Y. Wei and Z. D. Jiang, *Mater. Sci. Semicond. Process.*, 105 (2020) 104708.
13. G. Gasparotto, J. P. C. Costa, P. I. Costa, M. A. Zaghete and T. Mazon, *Mater. Sci. Eng., C*, 76 (2017) 1240.

14. A. Pruna, Q. Shao, M. Kamruzzaman, J. A. Zapien and A. Ruotolo, *Electrochim. Acta*, 187 (2016) 517.
15. F. Li, R. X. Li, Y. Feng, T. Gong, M. Z. Zhang, L. Wang, T. J. Meng, H. X. Jia, H. Wang and Y. F. Zhang, *Materials Science and Engineering: C*, 95 (2019) 78.
16. P. Saha, J. W. Hill, J. D. Walmsley and C. M. Hill, *Anal. Chem.*, 90 (2018) 12832.
17. W. Q. Zhang, Y. Lu, T. K. Zhang, W. P. Xu, M. Zhang and S. H. Yu, *Journal of Physical Chemistry C*, 112 19872.
18. B. Q. Sun and H. Sirringhaus, *Nano Lett.*, 5 (2005) 2408.
19. B. Q. Sun and H. Sirringhaus, *J. Am. Chem. Soc*, 128 (2006) 16231.
20. Y. Y. Zhang, Y. Y. Wang, K. B. Wu, S. C. Zhang, Y. Zhang and C. D. Wan, *Colloids Surf. B. Biointerfaces*, 103 (2013) 94.
21. H. Gu , Y. Yang , J. X. Tian and G. Y. Shi, *ACS Appl. Mater. Interfaces*, 5 (2013) 6762.
22. P. Roy, A. P. Periasamy, C. T. Liang and H. T. Chang, *Environ. Sci. Technol.*, 47 (2013) 6688.
23. F. X. Ma, J. Wang, F. B. Wang and X. H. Xia, *Chem. Commun.*, 51 (2015) 1198.
24. L. B. Tang , R. B. Ji , X. M. Li , K. S. Teng and S. P. Lau, *Part. Part. Syst. Charact.* , 30 (2013) 523.
25. J. D. Qiu, L. Shi, R. P. Liang, G. C. Wang and X. H. Xia, *Chemistry - A European Journal*, 18 (2012) 7950.
26. H. Li, S. S. Chu, Q. Ma, Y. Fang, J. P. Wang, Q. D. Che, G. Wang and P. Yang, *ACS Appl. Mater. Interfaces*, 11 (2019) 8601.
27. A. K. Zak, N. S. A. Aziz, A. M. Hashim and F. Kordi, *Ceram. Int.*, 42 (2016) 13605.
28. A. Janotti and C. G. Van de Walle, *Appl. Phys. Lett.*, 87 (2005) 122102.
29. J. F. S. Fernando, M. P. Shortell, K. L. Firestein, C. Zhang, K. V. Larionov, Z. I. Popov, P. B. Sorokin, L. Bourgeois, E. R. Waclawik and D. V. Golberg, *Langmuir*, 34 (2018) 7334.
30. X. Fang, J. F. Liu, J. Wang, H. Zhao, H. X. Ren and Z. X. Li, *Biosensors Bioelectron.*, 97 (2017) 218.
31. A. Zabihollahpoor, M. Rahimnejad, G. Najafpour and A. A. Moghadamnia, *J. Electroanal. Chem.*, 835 (2019) 281.
32. K. Sheng, L. Wang, H. C. Li, L. Zou and B. X. Ye, *Talanta*, 164 (2017) 249.
33. E. Laviron, *J. Electroanal. Chem.*, 52 (1974) 355.
34. J. L. Wang, J. e. Huo, J. Li, E. Shangguan and Q. M. Li, *Anal. Methods*, 5 (2013) 4119.
35. Z. B. Wang, J. X. Hu, H. X. Du, S. He, Q. Li and H. Q. Zhang, *J. Pharm. Biomed. Anal.*, 125 (2016) 178.